Pattern formation in the flow of thin films down an incline: Constant flux configuration

L. Kondic[a] and J. Diez[b]

Department of Mathematical Sciences and Center for Applied Mathematics and Statistics, New Jersey Institute of Technology, Newark, New Jersey 07102

We present fully nonlinear time-dependent simulations of a thin liquid film flowing down an inclined plane. Within the lubrication approximation, and assuming complete wetting, we find that varying the inclination angle considerably modifies the shape of the emerging patterns: Finger-shaped patterns result for the flow down a vertical plane, while saw-tooth patterns develop for the flows down an inclined plane. However, in all of our simulations, the roots always move, indicating that the shape of the patterns is not necessarily related to the surface coverage, a technologically important feature of the flow. Furthermore, we find that triangular steady-state patterns may be produced for the flow down an incline, while the fingers typically grow in length for all explored times. We find quantitative agreement with reported experiments, and suggest new ones. © *2001 American Institute of Physics.* [DOI: 10.1063/1.1409965]

I. INTRODUCTION

The flow of thin films is relevant in a number of different fields, such as engineering (microchip production), biology (lining of mammalian lungs), and chemistry (flow of surface active materials). These flows can be driven by gravitational (flow down an inclined plane), centrifugal (spin coating), or Marangoni forces. In all these different settings, the front dynamics is not completely understood. In many situations, the fluid fronts become unstable, leading to finger-like rivulets, triangular saw-tooth patterns, or, in the case of surfactant flow, dendritic tip-splitting petals. Very often, these instabilities are undesirable in technological applications, since they may lead to the formation of dry regions. From a more fundamental viewpoint, one wishes to understand the dynamics of these strongly nonlinear systems, and reach general conclusions concerning instabilities.

In this work, we concentrate on perhaps the simplest of these problems, the flow of a thin film down an inclined plane. Experiments are usually performed by releasing a constant (fixed) volume of fluid at the top of an incline. After some time, the initially straight contact line, where liquid, gas, and solid phase meet, becomes unstable with respect to transverse perturbations. It has been conjectured that this instability is related to the formation of a capillary ridge in the fluid profile, just behind the advancing contact line. While the initial stages of the instability process are rather well understood, as outlined below, it is still not clear what determines the long-time nature of the instability, in particular the shape of the patterns and the degree of surface coverage. The work by Silvi and Dussan,[1] expanding on the pioneer work by Huppert,[2] shows that the wetting properties of the fluid play an important role: They obtain triangular patterns and complete surface coverage for an (almost) completely wetting fluid, while finger-shaped patterns and partial surface coverage result for a partially wetting fluid. Jerret and de Bruyn[3] and De Bruyn[4] obtain results consistent with Silvi and Dussan[1] and Huppert,[2] and further quantify them by measuring the manner in which the patterns grow. More recent works by Veretennikov, Indeikina, and Chang,[5] Hocking, Debler, and Cook,[6] Johnson,[7] and Johnson, Schluter, Miksis, and Bankoff[8] show that the problem is more complicated than previously thought. Veretennikov *et al.*[5] perform experiments on both dry and prewetted surfaces and obtain different patterns in these two cases. They also report that a partially wetting fluid characterized by a large contact angle can form an overhanging ''nose'' at the contact line, in contrast to the ''wedge'' profile typical for more wetting fluids. Hocking *et al.*[6] observe both triangular and finger shaped patterns with a single fluid–solid configuration. Johnson[7] and Johnson *et al.*[8] modify the experimental setup to allow for a continuous flow of fluid, referred in what follows as ''constant flux'' configuration, compared to ''constant volume'' in all other experiments. An example of their experimental results is shown in Fig. 1: For a given fluid–solid combination, changing the inclination angle of the substrate can have significant effects on the shape of the emerging patterns. More details about the experimental parameters are given in Sec. IV B.

Theoretical analysis of the problem requires, in the first place, resolving the so-called ''contact line paradox.'' As it is well known, assuming standard no-slip boundary condition at the contact line leads to a multivalued velocity field there (see, e.g., Dussan,[9] de Gennes,[10] or Haley and Miksis[11]). This problem is typically approached by either relaxing the no-slip boundary condition, or assuming the presence of a thin precursor film in front of the propagating contact line. Both approaches introduce a short length scale into the problem, thus requiring analysis of the influence of this additional parameter on the instability.

---

[a]Electronic mail: kondic@m.njit.edu
[b]Permanent address: Instituto de Física Arroyo Seco, Universidad Nacional del Centro de la Provincia de Buenos Aires, Pinto 399, 7000, Tandil, Argentina. Electronic mail: jdiez@exa.unicen.edu.ar
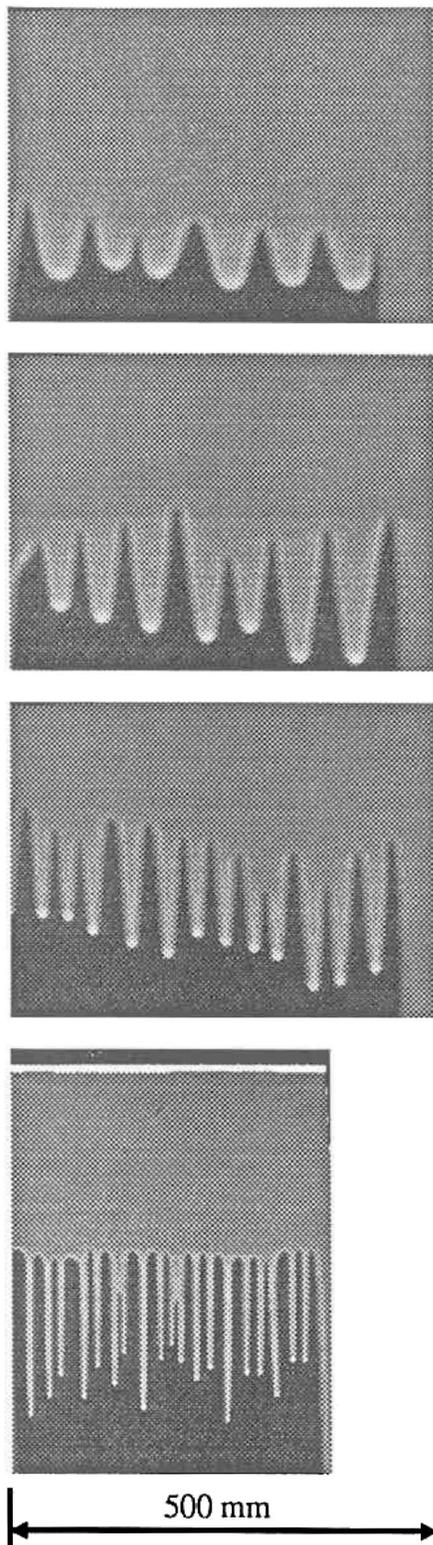
FIG. 1. Patterns formed in constant flux experiment by Johnson (Ref. 7). The fluid is glycerine–water mixture (more details about this experimental setup are given in Sec. V B), and the inclination angle is (from top to bottom) α=7.2°, 13.9°, 27.9°, and 90.0°. The profiles are shown after the fluid traveled the same distance down an incline. (Reproduced with permission of the author.)

The dynamics of the main body of the fluid film is typically approached within the framework of the lubrication approximation. Goodwin and Homsy[12] show that this approach is appropriate for completely wetting fluids, while in

the case of partially wetting fluids some of the assumptions of the lubrication approach might be violated at the contact line. López, Miksis, and Bankoff[13] analyze the effect of neglected inertial terms, and show that their influence on the instability is rather weak, even for O(1) Reynolds numbers. Consistently, the experiments by Johnson et al.,[8] where Reynolds number of the flow is systematically varied, show relatively little effect of fluid inertia on the pattern formation process.

An initial insight into the instability results from the linear stability analysis (LSA), within the framework of the lubrication approximation. Troian et al.[14] perform LSA for the flow down a vertical plane and show that there is a band of unstable modes, with short wavelengths stabilized by surface tension. Bertozzi and Brenner[15] extend the analysis to the general case of the flow down an inclined plane, and show that the normal component of gravity (hydrostatic term) shifts the mode of maximum growth to longer wavelengths, and also tends to stabilize the flow by decreasing the growth rate of the instability. While a basic agreement with the experimental results has been reached (e.g., the observed separation between the tips of the patterns agrees reasonably well with the wavelength of the mode of maximum growth, λ_m), there are a number of unanswered questions. Most importantly, LSA is limited to the early times evolution of a single mode, so that the questions concerning the long time evolution and the nonlinear mode interaction cannot be addressed. Some of these restrictions have been relaxed by a weakly nonlinear analysis by Kalliadasis.[16] That work explains the contact line instability as a phase instability related to the translational invariance of the system in the streamwise direction, and predicts a strong influence of the precursor film thickness: A large precursor film suppresses instability, in agreement with the experimental results by Veretennikov et al.[5] and Ye and Chang.[17]

There have been relatively few works that approached this problem from the computational point of view. The reason for this is that, even within the framework of lubrication approximation, there are still significant computational obstacles to overcome. Some of these are the stiffness introduced in the evolution equations by surface tension, and the need to resolve short length-scales close to the advancing contact line. The simulations by Schwartz[18] concentrate on the case of a completely wetting fluid, and show that triangular patterns result in that case. Moyle, Chen, and Homsy[19] develop more general simulations of partially wetting fluids, showing that the shape of the patterns can be modified by fluid wetting properties. Very recently, Eres, Schwartz, and Roy[20] perform the simulations where they appear to reach a nontrivial traveling wave (i.e., a steady flow configuration characterized by a nonuniform structure in the spanwise direction) for the flow of a completely wetting fluid down a vertical plane.

In this work we concentrate on the flow of a completely wetting fluid, and analyze the influence of the inclination angle on two most relevant aspects of the instability: Shape of the patterns, and surface coverage. An important motivation for analyzing the effect of this particular parameter comes from the fact that previous simulations of this prob-

lem have been performed only for the flow down a vertical plane, while the experiments concentrate on the flow down an (sometimes very slightly) inclined plane. In an earlier work, Diez and Kondic[21] present the basic outline of the influence of the inclination angle. That work is extended here to provide a more complete picture of the instability mechanism, including the discussion of possible formation of nontrivial traveling waves. To further facilitate comparison with experiments, we perform simulations in large computational domains that compare well with the experimental ones. In these simulations, we do not enforce the emerging wavelengths, as done previously,[18–20] but let the system choose the separation between patterns on its own. We note that in the experiments it is not obvious what kind of perturbation generates the instability. It might develop due to noise perturbing either the contact line itself, or the fluid–substrate interaction, or the body of the fluid far behind the contact line. Influence of the perturbations on the fluid–solid interaction has been recently analyzed by Bertozzi and Brenner,[15] Ye and Chang,[17] and Kondic and Bertozzi,[22] with the main goal of understanding the instabilities at small inclination angles. In this work we concentrate on the effects that perturbations of the contact line itself have on the development of the instability, and consider perturbations of the substrate only briefly at the end of Sec. IV. For clarity, we limit the discussion to the situation corresponding to the experimental setup of Johnson et al.,[8] where there is a constant flux of the fluid far behind the contact line. Correspondingly, we do not discuss the issues related to thinning of the fluid that occurs if a constant volume of fluid is let to flow down an incline. The main goals of the present work are to (1) establish quantitative connection between theoretical work and experimental observations, and (2) provide computational results that will serve as a guide to future research on more fundamental issues, such as nonlinear mode interaction, and the possible existence of nontrivial traveling wave solutions.

This paper is organized as follows. First, in Sec. II we explain the main features of the theoretical approach and the numerical scheme. In Sec. III we then present the results of the one-dimensional (1D) simulations, where the fluid front is assumed to be straight in the transverse direction. The results of the simulations in domains whose lateral size is close to the wavelength of maximum growth and equal to the perturbation wavelength are presented in Sec. IV, where we also analyze the influence of the parameters (in particular, precursor film thickness and inclination angle) on the long-time dynamics of the evolving patterns. Next, in Sec. V, we study the effects of the domain size and of the nonlinear mode interaction on the resulting patterns. The narrow domain results allow for a better insight into the fundamental issues related to the instability, and the results of the simulations performed in wide domains allow for direct comparison with experimental observations. Finally, Sec. VI is devoted to conclusions and final remarks.

II. FORMULATION OF THE PROBLEM AND NUMERICAL METHODS

Within the framework of the lubrication approximation, the velocity of the fluid is depth-averaged over the thickness of the film (see, e.g., Greenspan[23]). Following this approach, one obtains the average fluid velocity, $\mathbf{v}=(u,v)$,

$$\mathbf{v}=-\frac{h^2}{3\mu}[\nabla p-\rho g\sin\alpha\,\mathbf{i}], \qquad (1)$$

where $\nabla=(\partial_x,\partial_y)$, h is the fluid thickness, p is the pressure, μ is the viscosity, ρ is the density, g is gravity, and α is the inclination angle of the plane of the substrate. The coordinate frame is chosen so that $\mathbf{i}$ points down the incline, and $\mathbf{j}$ is the transverse direction in the plane. We note that Eq. (1) assumes no-slip boundary condition at the fluid–solid interface. The pressure includes the hydrostatic component, and the contribution following from the Laplace–Young boundary condition at the fluid–air interface

$$p=-\gamma\nabla^2h+\rho gh\cos\alpha, \qquad (2)$$

where γ is the surface tension. Assuming fluid incompressibility, the continuity equation gives

$$\frac{\partial h}{\partial t}=-\nabla\cdot(h\mathbf{v})$$

$$=-\frac{1}{3\mu}\nabla\cdot[\gamma h^3\nabla\nabla^2h-\rho gh^3\nabla h\cos\alpha+\rho gh^3\sin\alpha\,\mathbf{i}]. \qquad (3)$$

Thus, the lubrication approximation reduces Navier–Stokes equations to this nonlinear fourth order partial differential equation that governs the time evolution of the film thickness $h(x,y,t)$. To balance viscous and capillary forces in Eq. (3), we scale h by the fluid thickness far behind the contact line, h_c, and define the scaled in-plane coordinates and the time by $(\bar{x},\bar{y},\bar{t})=(x/x_c,y/x_c,t/t_c)$, where

$$x_c=\left(\frac{a^2h_c}{\sin\alpha}\right)^{1/3}, \quad t_c=\frac{3\mu}{\gamma}\frac{a^2x_c}{h_c^2\sin\alpha}, \qquad (4)$$

and $a=\sqrt{\gamma/\rho g}$ is the capillary length. The velocity scale is chosen naturally as $U=x_c/t_c$, and the capillary number is defined as $Ca=\mu U/\gamma$. Using this nondimensionalization, Eq. (3) for $\bar{h}=h/h_c$ is given by (dropping the bars)

$$\frac{\partial h}{\partial t}+\nabla\cdot[h^3\nabla\nabla^2h]-D(\alpha)\nabla\cdot[h^3\nabla h]+\frac{\partial h^3}{\partial x}=0, \qquad (5)$$

where the single dimensionless parameter $D(\alpha)=(3Ca)^{1/3}\cot(\alpha)$ measures the size of the normal component of gravity. We note that the lubrication approximation requires the slope of the free surface to be small; assuming slopes of O(1) in terms of our nondimensional variables, this implies $[(h_c/a)\sqrt{\sin\alpha}]^{2/3}\ll 1$.[14] For small α's, this condition is always fullfiled; however, for large α's, it is valid only for very thin films, such as those in Johnson et al.,[8] where $h_c/a\approx 0.2$. We concentrate on this situation and assume in the rest of this work that the lubrication approximation is valid.

As mentioned in the Introduction, all the theoretical and computational methods require some regularizing mechanism—either assumption of a small foot of fluid in front of the apparent contact line (precursor film, see the works by Troian et al.,[14] Bertozzi and Brenner,[15] or Spa and

Homsy[24]), or relaxing the no-slip boundary condition at fluid–solid interface (see e.g., Greenspan,[23] Dussan,[26] or Hocking and Rivers[27]). Diez, Kondic, and Bertozzi[28] have recently performed an extensive analysis of the computational performance of these regularizing mechanisms applied to the spreading drop problem. In that paper it is shown that the results are rather insensitive to the choice of the model, consistently with, e.g., Spa and Homsy.[24] However, the computational performance of the precursor film model is shown to be much better than that of various slip models. For this reason, we also use a precursor film of thickness b (scaled by h_c) as a regularizing method in this work.

The computational domain is chosen as a rectangle defined by $0 \leqslant x \leqslant L_x$ and $0 \leqslant y \leqslant L_y$ which is divided into $N_x \times N_y$ node points (x_i, y_j) with $i = 1, \ldots, N_x$ and $j = 1, \ldots, N_y$. Equation (5) is then discretized in space using a central finite difference scheme leading to the following system of equations for $h_{i,j}$ [that is, the numerical approximation to $h(x_i, y_j, t)$]

$$\frac{dh_{i,j}}{dt} + f_{i,j} = 0; \quad i = 1, \ldots, N_x; \quad j = 1, \ldots, N_y, \qquad (6)$$

where $f_{i,j}$ is a nonlinear operator which depends on the values of h at the neighboring grid points.

Let us concentrate for a moment on the capillary term, and define the diffusivity $\mathcal{D} = h^3$. To obtain a numerical approximation for $f_{i,j}$, we need $\mathcal{D}_{i \pm 1/2, j}$ and $\mathcal{D}_{i, j \pm 1/2}$. These quantities can be obtained by interpolation. While there are various (second-order correct) ways in which this interpolation can be done, Zhornitskaya and Bertozzi[29] and Zhornitskaya,[30] building upon the work by Bernis and Friedman,[31] show that one particular interpolation leads to a scheme which is positivity preserving, i.e., the solution which is strictly positive for $t = 0$ preserves this property for all times. Diez et al.[28] compare the performance of this scheme to the one based on standard interpolation, and find that it has significant computational advantages. We also use this scheme here, and interpolate the diffusivity $\mathcal{D}_{i+1/2, j}$ by

$$\mathcal{D}_{i+1/2, j} = \begin{cases} \dfrac{h_{i+1,j} - h_{i,j}}{g_{i+1} - g_i}; & h_{i+1,j} \neq h_{i,j} \\ h_i^3; & h_{i+1,j} = h_{i,j} \end{cases}, \qquad (7)$$

where $g(h)$ is defined by $g''(h) = 1/\mathcal{D}(h)$. Analogous expression is used for $\mathcal{D}_{i, j+1/2}$.

The two gravitational terms in Eq. (5) are discretized using standard centered finite differences. In the normal gravity term we use

$$(h^3)_{i+1/2, j} = \frac{h_{i+1,j}^3 + h_{i,j}^3}{2}, \qquad (8)$$

with analogous expression for $(h^3)_{i, j+1/2}$. In the parallel gravity term we discretize as

$$\left(\frac{\partial h^3}{\partial x} \right)_{i,j} \approx \frac{1}{4 \Delta x_i} [(h_{i+1,j}^2 + h_{i,j}^2)(h_{i+1,j} + h_{i,j})$$
$$- (h_{i,j}^2 + h_{i-1,j}^2)(h_{i,j} + h_{i-1,j})]. \qquad (9)$$

The boundary conditions are chosen to model constant fluid flux, $\Phi = h\mathbf{v}$, far behind the contact line. To this effect, we set the boundary condition at $x = 0$ as $\partial \Phi_x / \partial x = 0$ for $0 \leqslant y \leqslant L_y$, where $\Phi_x = hu$ is the x-component of Φ. The same boundary condition is also applied at $x = L_x$. Thus, $h_{1,j}$ as well as $h_{N_x, j}$ ($j = 1, \ldots, N_y$) remain constant in time. This is enforced by setting $f_{1,j} = f_{N_x, j} = 0$ [see Eq. (6)]. At the boundaries $y = 0$ and $y = L_y$ ($0 \leqslant x \leqslant L_x$), we have a no-flow boundary condition, $\Phi_y = 0$. One choice that satisfies this constraint [see Eq. (3)] is

$$\frac{\partial h}{\partial y} = \frac{\partial^3 h}{\partial y^3} = 0, \quad \text{at} \quad y = 0, L_y, \quad 0 \leqslant x \leqslant L_x. \qquad (10)$$

Other boundary conditions can be chosen; we use those specified by Eq. (10) due to their simplicity, and due to the fact that they are applicable to a wide variety of problems. We note that only the normal component of the flux, Φ_y, is set to zero at $y = 0, L_y$, while the tangential component, Φ_x, is let free, so that these boundaries can be thought of as "slipping walls." Since odd derivatives are set to zero there, they can be also considered as symmetry planes.

Time discretization is performed using implicit Crank–Nicolson scheme. The advantages of the implicit scheme for this problem are obvious: The stability requirement for an explicit scheme is that $\Delta t < C \min[\Delta x, \Delta y]^4$, where Δt is a time step, and C is a positive constant. Thus, an explicit scheme requires very short time steps for a reasonable spatial accuracy.

To explain time discretization, it is convenient to substitute $k = i + (j-1)N_x$, where $i = 1, \ldots, N_x, j = 1, \ldots, N_y$ in the system of ordinary differential equations, Eq. (6). Applying Crank–Nicolson scheme to this system, and using the notation h_k^ν to denote the solution at the point k at the time t^ν, leads to the system of $N_{xy} = N_x \times N_y$ nonlinear algebraic equations

$$\frac{h_k^{\nu+1} - h_k^\nu}{\Delta t^\nu} + \frac{1}{2} (f_k^{\nu+1} + f_k^\nu) = 0 \quad (1 \leqslant k \leqslant N_{xy}), \qquad (11)$$

where Δt^ν is a νth variable time step, and $t^\nu = \nu \Delta t^\nu$. This system is linearized using the Newton–Kantorovich method; the linearized problems are then solved using iterative biconjugate gradient method.

Time evolution from a given initial condition (discussed in the next section) is performed by variable time steps, the size of which is limited by two requirements: (a) That the solution is strictly positive everywhere in the domain, and (b) that an accuracy condition is satisfied. The condition (b) is enforced by estimating the local relative error e_k of the solution $h_k^{\nu+1}$. A Taylor expansion around h_k^ν leads to

$$e_k = \frac{(\Delta t^\nu)^2}{h_k^\nu} \frac{d^2 h_k^\nu}{dt^2}, \qquad (12)$$

so that

$$e_k \approx \frac{2 \Delta t^\nu}{\Delta t^{\nu-1}} \frac{\Delta t^{\nu-1} h_k^{\nu+1} + \Delta t^\nu h_k^{\nu-1} - (\Delta t^{\nu-1} + \Delta t^\nu) h_k^\nu}{(\Delta t^{\nu-1} + \Delta t^\nu) h_k^\nu}. \qquad (13)$$
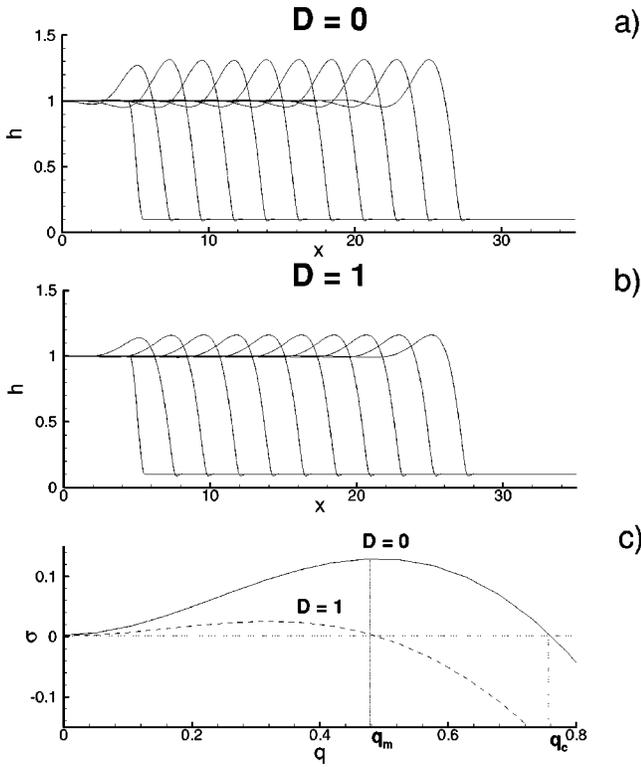
FIG. 2. Profiles of a film flowing down a vertical plane (a), and down an inclined plane (b). The time interval between profiles is $\delta t = 2$, the grid size is $\Delta x = 0.05$, and $b = 0.1$. (c) Growth rate σ following from LSA vs wave number $q = 2\pi/\lambda$ for $D = 0$ and $D = 1$. The wavelength of maximum growth is $\lambda_m = 2\pi/q_m$, and the critical wavelength is $\lambda_c = 2\pi/q_c$.

FIG. 3. Fluid thickness and velocity profile of the film near the apparent contact line for $D = 1$ and $b = 0.1$.

If $E = \max(e_k)$ ($1 \leq k \leq N_{xy}$) is less than a given upper bound E_m (typically, $E_m = 10^{-2} - 10^{-3}$), the solution $h_k^{\nu+1}$ obtained with the time step Δt^ν is accepted; otherwise, Δt^ν is reduced and a new calculation of $h_k^{\nu+1}$ is performed.

The simulations that follow are computationally intensive, so that significant effort has been put in producing an efficient method. To illustrate this point, we note that larger simulations presented in Sec. V, are typically performed using about 10^5 grid points. Spatial discretization then leads to a system of 10^5 nonlinear algebraic equations [Eq. (6)]. After linearization, one needs to invert a sparse $10^5 \times 10^5$ matrix with about 10^6 nonzero elements. Any direct approach to solving this problem would be too slow; for that reason an iterative method is chosen. Furthermore, time accuracy requirement limits the time step to about 10^{-2}, requiring about 10^4 time steps for a typical simulation. The computing times on the fastest available workstations (R12000 CPU) vary between 15 and 20 hours for the smaller simulations in Sec. IV, to a couple of weeks for larger simulations presented in Sec. V.

III. ONE-DIMENSIONAL SOLUTION AND LINEAR STABILITY ANALYSIS

Let us for a moment ignore contact line instability, and remove the y-dependence of the fluid profile from the problem. Figures 2(a) and 2(b) then show snapshots of the fluid profiles at equal time intervals for $D = 0$ and $D = 1$, resulting from these 1D simulations (recall that $+x$ direction points down the incline). We see that, after initial transients, the flow develops a traveling wave profile, that moves with the constant velocity $v_f = 1 + b + b^2$ (see, e.g., Bertozzi and Brenner[15]).

The main feature of the profile $h(x,t)$ is the presence of a bump near the contact line. This bump, resulting from the fluid accumulation behind the front, is due to the fact that the viscous stress on the plane is much greater in the contact line region than in the fluid bulk. The increased viscous stress is balanced by the component of the bump weight in the downslope direction. Linear stability analysis[14,15,24] obtains that the presence of the bump is a necessary condition for the instability of the fluid to small perturbations in the transverse direction. Our LSA result for the parameters used in Figs. 2(a) and 2(b), are shown in Fig. 2(c). The growth rate σ, calculated as the eigenvalue of the linearized problem,[14,15,24] is consistent with the previous results. An increase of D leads to a decrease in the growth rates, and also to a shift of the mode of maximum growth (characterized by $\lambda_m = 2\pi/q_m$, where $\sigma(q_m) = \max|\sigma(q)|$), to longer wavelengths; we relate this prediction to our 2D simulations later in Sec. V. We also note that the height of the bump and LSA results depend on the precursor thickness: smaller b leads to larger bump, and stronger instability. This effect is discussed in more detail in Sec. IV.

Remark:

There is an interesting feature of the fluid flow in the contact line region, shown (magnified) in Fig. 3(a). We see the formation of a fluid depression (dip) ahead of the front region, which leads to a local negative velocity field [Fig. 3(b)]. (Dip formation can be also seen in the previous simulations of this problem,[20,24] but, to our knowledge, it has not been analyzed in any detail.) The fluid within the precursor film (which is flowing down with the velocity equal to b^2) is sucked into the bulk region due to a decrease in capillary pressure, and later pushed in the positive direction again. This negative velocity field can be understood based on mass conservation. In the moving reference frame (moving with v_f), the flux in the x direction is given by $\Phi_x = h(v - v_f) = -b(b + 1)$, where the last equality can be obtained by calculating the flux far in front of the contact line.[14,15,24,32] Since in the dip region $h < b$, we write $h = \theta b$, $\theta < 1$, and obtain

$$v = b^2 - (b+1)\frac{(1-\theta)}{\theta}. \tag{14}$$

Thus, $v < 0$, provided $\theta < (b+1)/(1+b+b^2)$. Our simulations show that, for any typical b, h in the dip region is small enough ($\theta \approx 0.85$) to produce negative velocities there.

We note that this depression was first noted in Ref. 33 in the context of drop spreading on a horizontal pre-existing film. It is a purely surface tension effect; we have noticed only very weak influence of the forcing gravity term in $+x$ direction on its magnitude.

IV. EVOLUTION OF A SINGLE TRANSVERSE MODE

In this section we address the problem of the dynamics of a thin film contained in a domain whose lateral dimension is comparable to the wavelength of maximum growth from LSA, and to the domains used in previous simulations of this problem.[18–20] We compare our results with those simulations, as well as with experimental results,[7,8] and linear[14,15,24] and weakly nonlinear[16] stability analyses. As a representative case, we use $L_y = 16$.

A. Vertical plane ($D=0$)

The simulations are performed using as initial condition the results of 1D simulations, perturbed at $t=0$ by a single transverse mode characterized by the wavelength $\lambda_0 = L_y$. The position of the front at $t=0$ is then given by

$$x_f(y) = x_{f0} - A_0 \cos(2\pi y/\lambda_0), \tag{15}$$

where x_{f0} is the unperturbed position (see also Diez and Kondic[21]). The perturbation is characterized by a small amplitude A_0, and a phase such that this initial condition satisfies $\partial h/\partial y = 0$ at $y = 0, L_y$. We have verified that without imposed perturbation, the flow evolves for very long times ($t > 1000$) without deforming the front line, thus indicating that numerical noise alone (possibly due to roundoff error) does not lead to instability at the time scales considered in this work. Most of the computations are performed using a precursor film of thickness $b = 0.01$, on the grid $\Delta x = 0.2$, $\Delta y = 0.25$. The convergence studies show that this grid spacing is sufficient (convergence results follow). The size of the computational domain is typically varied between $L_x = 40$ and $L_x = 60$, except in the case of simulations extended to very long times, presented in Sec. IV C, where $L_x = 200$. Since the computations are performed in the laboratory frame, the computational box is shifted when necessary in the direction of the flow. Alternatively, one can perform computations in the reference frame moving with the velocity of the unperturbed flow, v_f; this corresponds to shifting the box at each time step. We have verified that these two approaches lead to consistent results.

Figure 4 shows the flow at four different times. Since at $t=0$ only a single (linearly unstable) wavelength is present, this one grows and forms a long finger with almost straight sides, resembling the shape of the patterns observed by Johnson et al.,[8] and reproduced in Fig. 1 (note that Fig. 4 is significantly stretched in the y direction).
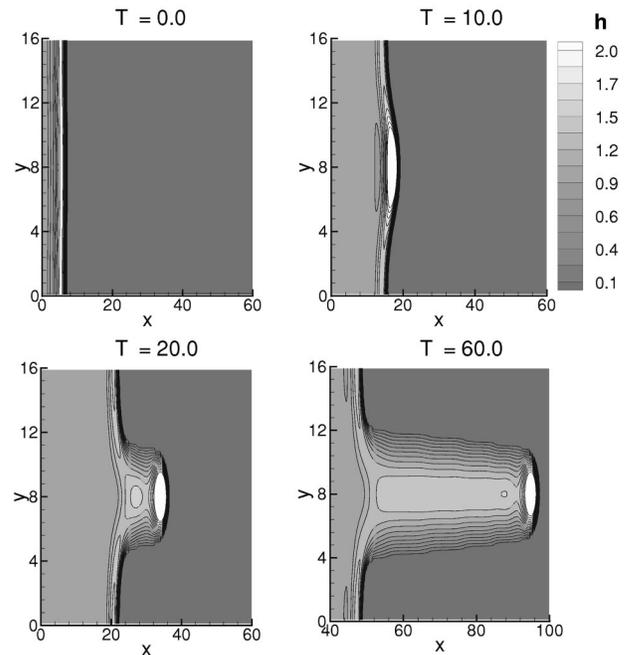
FIG. 4. Contour plot of the flow down a vertical plane perturbed by a single mode characterized by $A_0 = 0.1$ and $\lambda_0 = 16$. The precursor film thickness is $b = 0.01$, and the grid spacing is $\Delta x = 0.2$, $\Delta y = 0.25$.

To follow the development of the instability more quantitatively, we record the position of the tip, x_t, and the position of the root, x_r, as a function of time (recall that the boundaries $y = 0, L_y$ can be considered as slipping walls). Figure 5(a) shows that there is a rather fast growth of the pattern for very early times, followed by a slower growth for later times. For these later times, the velocities of propagation of the tip, v_t, and the root, v_r, are approximately constant: $v_t \approx 1.55$, $v_r \approx 0.7$ (the velocity of the unperturbed front is $v_f \approx 1$). From these results, we extract the length $L(t) = x_t - x_r$ of the finger as a function of time. Figure 5(b) shows this quantity normalized by the initial length $L_0 = 2A_0$ on a semilog graph. For early times, $L(t)$ increases exponentially with the growth rate σ [defined by $L(t)/L_0$
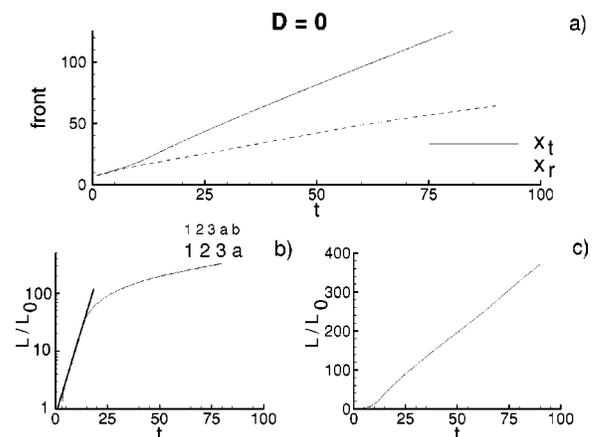
FIG. 5. (a) The positions of the tip and root as function of time. (b) The length of the finger normalized by the initial length $L_0 = 2A_0 = 0.2$ on semilog scale; the straight line has a slope of 0.235 as explained in the text. (c) The result from (b) on linear scale. The parameters are as in Fig. 4.

TABLE I. The table gives the results for the (nondimensional) width, length, and growth rates of the patterns for different Δx, Δy, and the parameter E_m, that determines accuracy of the time evolution; all other parameters are as in Fig. 4. The widths are defined as full widths of the patterns at half length; the results are given at time $t=17$.

Δx	Δy	E_m	width	length	σ
0.1	0.125	10^{-2}	9.0	10.6	0.234
0.1	0.25	10^{-2}	9.2	10.8	0.235
0.1	0.5	10^{-2}	10.0	11.4	0.238
0.2	0.125	10^{-2}	9.0	10.8	0.235
0.2	0.25	10^{-2}	9.2	11.0	0.235
0.2	0.5	10^{-2}	9.8	11.5	0.238
0.4	0.125	10^{-2}	9.6	6.4	0.204
0.4	0.25	10^{-2}	10.2	6.5	0.205
0.4	0.5	10^{-2}	10.4	6.8	0.207
0.2	0.25	10^{-4}	9.2	11.0	0.235
0.2	0.25	10^{-3}	9.2	11.0	0.235
0.2	0.25	10^{-2}	9.2	11.0	0.235
0.2	0.25	10^{-1}	9.6	11.2	0.237
0.2	0.25	1.0	9.6	11.4	0.238

FIG. 6. Influence of the precursor thickness b on (a) length of the finger, (b) position of the tip, and (c) position of the root. Other parameters are as in Fig. 4. The arrows show the direction in which b is increased.

$=\exp(\sigma t)]$ determined to be $\sigma \approx 0.235$, very close to its value predicted by LSA (for $\lambda \approx 14$, Troian *et al.*[14] obtain $\sigma_m \approx 0.24$). Figure 5(c) shows the same result on a linear graph, which is more convenient for late times. For the time range shown in this figure, we see linear increase of the finger length. The transition between exponential and linear growth is explained qualitatively by Brenner,[25] who estimates that this transition happens when the length of the pattern becomes comparable to the width of the capillary ridge. By comparing Fig. 5(b) with Fig. 2(a), which shows the profile of the unperturbed front, we see that the computational results agree well with this estimate. The question of growth for very long times is discussed later in Sec. IV C, in the more general context of the flow down an inclined plane. In the remainder of this section we analyze the influence of the parameters used in our computations.

First, we verify that the discretization parameters—grid size and time step—produce sufficiently accurate results. The main characteristics of the solution we want to check are the widths, lengths, and growth rates of the patterns. These results are shown in Table I for relatively early times, so that we can also compare the results for the growth rates with LSA. (Convergence studies are also performed for long times, with very similar results.) Table I shows that the results calculated on a grid $\Delta x \leq 0.2$, $\Delta y \leq 0.5$ agree very well with the LSA results; larger Δx leads, however, to a considerable error. We note that the time accuracy is kept fixed for the results shown in the first part of Table I, so that the convergence is not exactly quadratic. In the second part of the table we show the influence of the parameter E_m which determines the size of the time step through Eq. (13). For $E_m \leq 10^{-2}$, and $\Delta x = 0.2, \Delta y = 0.25$, the results are practically independent of this parameter. Again, due to the spatial discretization error, the convergence is not exactly quadratic. The results in Table I, as well as similar ones calculated for longer times, suggest our choice of the grid, $\Delta x = 0.2$ and $\Delta y = 0.25$ ($\Delta y = 0.5$ for the results in Sec. V B), and of the imposed time accuracy.
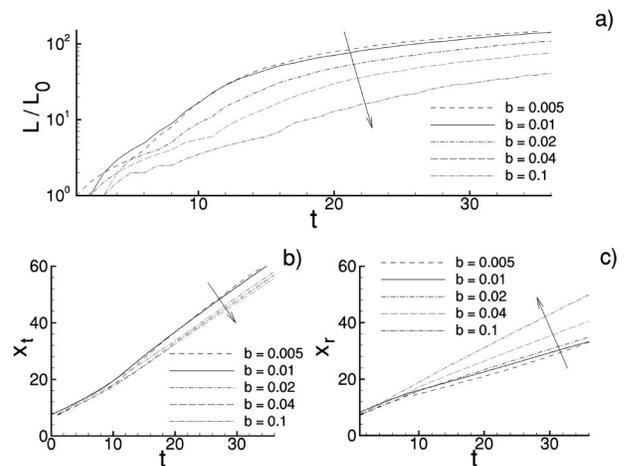
Next, we analyze the influence of the precursor film thickness on instability. Experimentally, it is possible to control the value of this parameter in flows on a prewetted substrate, as done systematically by Ye and Chang.[17] However, in most of the experiments, b is a rather small quantity, $b \approx 10^{-4} - 10^{-5}$. Such small values of b lead to computational difficulties, since the convergence issues require very fine grids and bring computational cost to an unacceptable level. Fortunately, from LSA[14,15,24] we know that the growth rates depend on b rather weakly. This is also confirmed by the weakly nonlinear analysis.[16] These results encouraged us to try to find the "optimal" value of b, so that the results that are of interest to us (such as growth rates) are computationally accurate, but also almost b-independent. In order to compare our results with LSA and experiments, we also explore the influence of relatively large b's on the instability.

Figure 6(a) shows the influence of b on the length of the pattern. We see that the growth rate of the patterns is significantly reduced for larger b's, in agreement with LSA results.[14,15,24] Figures 6(b) and 6(c) show the effect that larger b's have on the speed of tips and roots. As b's are increased, the tips move slower, while the roots move faster. The increase of the root velocities is as expected, since larger b's permit easier flow (less viscous stresses) in the root regions. Mass conservation then leads to slowing down of the tips. Thus, increase of b makes the velocities of tips and roots approach the velocity of the unperturbed planar front, from above and below, respectively. However, a decrease of b below 0.01 has much weaker influence: The speeds of both tips and roots (and the growth rates) become practically b-independent (see Fig. 6). This weak influence of b on the flow for $b \lesssim 0.01$ governed our choice of $b = 0.01$ in the simulations that we compare to experiments, characterized presumably by rather thin precursor films (or any other short lengthscale relevant in the vicinity of a contact line).

We note that for all explored b's, the speed of the roots is strictly positive. Since this speed is almost b-independent for small b's, we conjecture that this speed will be positive even for the b's relevant in the experiments. Correspond-

Phys. Fluids, Vol. 13, No. 11, November 2001

Pattern formation in the flow of thin films   3175
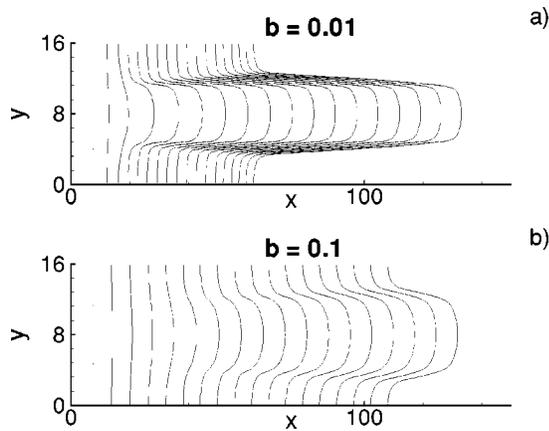
FIG. 7. Snapshots of the patterns in $\delta t = 5$ intervals for two representative b's: (a) $b = 0.01$, (b) $b = 0.1$. Other parameters are as in Fig. 4.

FIG. 8. Contour plot of the flow down an inclined plane ($D = 1$). All other parameters are as in Fig. 4.

ingly, our results suggest that complete coverage of the substrate eventually results.

The precursor thickness also influences the shape of the emerging pattern. Figure 7 show the snapshots of the patterns for two representative cases, $b = 0.01$ and $b = 0.1$. The profile obtained using $b = 0.01$ is characterized by almost straight sides, as observed in the experiments.[7,8] Larger b leads, however, to a pattern with more oblique sides. Additional simulations show that there is a continuous transition from almost straight to more oblique patterns as b is increased. For $b \lesssim 0.01$, the shape is almost insensitive to the value of b, similarly to the growth rates and to the speeds of tips and roots. Larger values of b in Eres *et al.*,[20] or, equivalently, larger slipping lengths in Moyle *et al.*,[19] might be the reason for obtaining more triangular-like pattern shapes in those simulations.

B. Inclined plane ($D > 0$)

We now proceed to the more general case of the flow down an inclined plane ($D > 0$). As a representative case, we choose $L_y = \lambda_0 = 16$, and $D = 1$.

Figure 8 shows the contours of the fluid height at four times. By comparing with Fig. 4, we see that the shape of the emerging pattern is very different. For $D = 0$, a finger with almost straight sides results; for $D = 1$, we obtain a pattern which much more closely resembles the triangular shapes seen in the experiments for the flow down an inclined plane[7,8] (see also Fig. 1). Another difference is that the development of the instability is much slower for $D = 1$ compared to $D = 0$, even in our nondimensional units [recall that the time scale $t_c \propto (\sin \alpha)^{-4/3}$, Eq. (4)].

Figure 9 shows the positions of the tips and roots for $D = 1$; for comparison, we also show the results for $D = 0$. In Fig. 9(a) we see that for $D = 1$, the tips move slower, and the roots faster, compared to $D = 0$, as observed experimentally by Johnson *et al.*[8] For $D = 1$, we still obtain exponential growth for early times, now characterized by a smaller growth rate $\sigma \approx 0.11$; a decrease of σ for larger D's is also predicted by LSA [viz. Fig. 2(c)]. For later times the growth slows down and becomes even slower than linear [Fig. 9(c)].
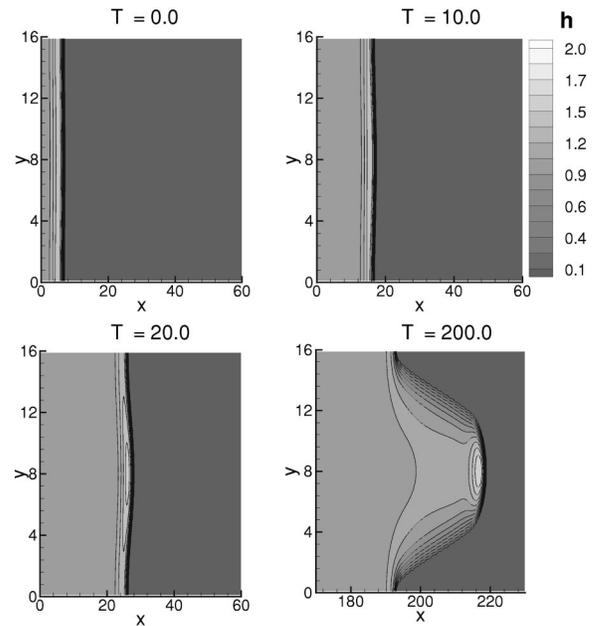
The possibility of growth saturation and steady solution for very long times is discussed below in Sec. IV C.

C. Long time dynamics

After the overview of the development of the instability, we now concentrate on the dynamics for very long times, aiming to understand the general features of the flow. The shapes of the emerging patterns do not change for longer times in any significant manner compared to the results shown in Figs. 4, 7, and 8. However, long time results give additional insight concerning increase of the pattern length.

Figure 10 shows that, for sufficiently large D's, growth saturation occurs. The growth saturates at smaller pattern lengths for larger D's, as one would expect, since an increase of D reduces the instability. We have verified that the satu-
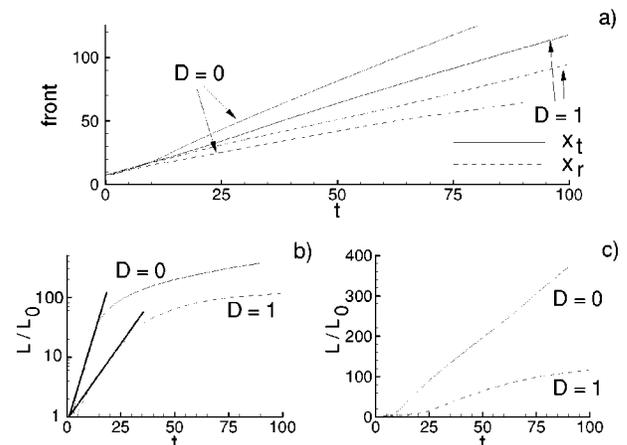
FIG. 9. (a) The positions of the fronts and roots as functions of time for $D = 0,1$. (b) The length of the patterns for $D = 0,1$. exponential fits for early times are also shown. (c) Results from (b) on linear scale. The parameters are as in Fig. 4 ($D = 0$) and Fig. 8 ($D = 1$).
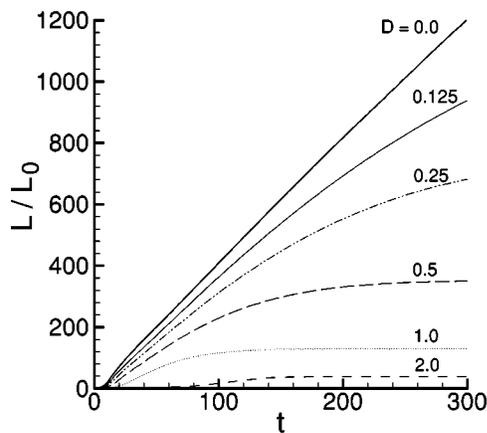
FIG. 10. Length of the emerging patterns for different D's. All other parameters are as in Fig. 4, except the box sizes in the x direction, which are $L_x = 200$.

FIG. 11. (a) Long time evolution of the length of the emerging patterns for $D=0$ and different b's. The solid lines emphasize the linear growth for $b=0.01$, and the deviation from linear growth for $b=0.1$. (b) Length of the emerging patterns for $D=0$ and different L_y's. All other parameters are as in Fig. 4, except the box sizes in the x direction, which are $L_x = 200$.

ration effect for $D>0$ is rather weakly influenced by the precursor thickness, the main effect being that, for a given D, larger b's lead to saturation at earlier times [see also Remark (4) below]. Additional convergence studies show that the saturation effect is not modified by grid refinement or by modifying the imposed time accuracy (effectively, changing the time step).

The growth saturation, that we obtain for larger D's, implies the existence of a stable nontrivial traveling wave solution, that results when the growth stops, and the fluid simply translates down the incline, without changing its shape. To our knowledge, this result has not been reported in the experimental literature. There are few possible explanations for this. First, most of the experiments are performed using constant volume configuration; possibly in that setup saturation does not occur. In the experiments where the constant flux configuration is used,[7,8] results for the time dependence of the patterns lengths are not reported; however, it appears that steady state profiles have not been observed.[34] Next, our simulations assume completely wetting fluid; the fluids used in the experiments are always partially wetting, even though the contact angle could be quite small. Finally, there is a possibility that saturation happens on a longer time scale than the one examined in the experiments. We present a detailed study of the experimental parameters and compare our nondimensional quantities with the experimental ones in Sec. IV B; here we just note that for the fluid properties of Fluid B,[8] and for the inclination angle corresponding approximately to $D=0.5$, our simulations predict saturated length of about 16 cm. This length compares rather well with the one shown in Johnson *et al.*[8] (see also Fig. 1). We consider that it would be of interest to perform experiments for even longer times in order to settle the question of existence of steady-state patterns. If saturation is not observed in experiments, then apparently this effect can be obtained only in the (ideal) case of a completely wetting fluid.

The question of growth saturation is also addressed computationally in the recent work by Eres *et al.*[20] They report saturation of growth in their simulations of a flow down a vertical plane, occurring at $t \approx 150$ (Fig. 14 in Ref. 20). This appears to be contradictory to our results for $D=0$ shown in Fig. 10. In order to understand this difference, we performed additional simulations of the $D=0$ case. In particular, we analyzed the effects of increasing–reducing time and space accuracy of our scheme, and the influence of varying the initial condition, without ever obtaining saturated solution for $D=0$. However, there are additional factors that can lead to modified results. One is the precursor film thickness, which is larger in Ref. 20, compared to the one used here. Figure 11(a) shows the difference in the results for the flow down a vertical plane and for very long times as b is increased: Growth becomes slower than linear for $t>100$. Still, at least for the times we explore, there is no saturation.
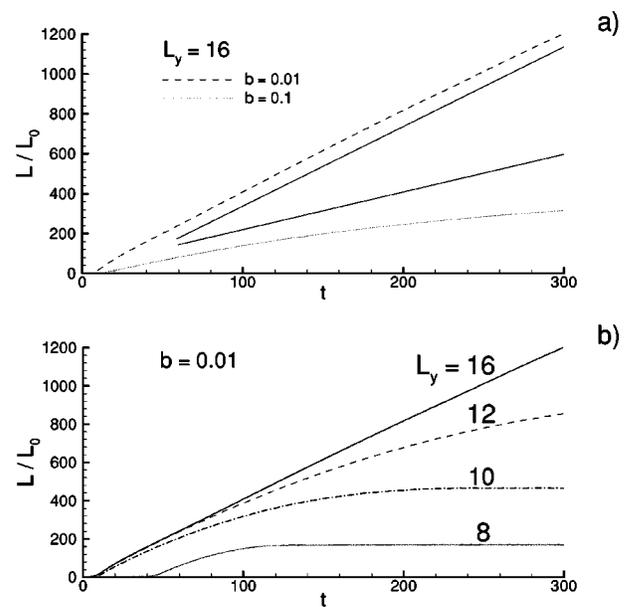
Another explanation of the different results is that the growth saturation (and the existence of a nontrivial traveling wave solution) may depend on the size of the computational domain in the transverse, y, direction. Indeed, Fig. 11(b) shows that this is really the case. In this figure we follow the pattern length for a few values of L_y and $D=0$ (recall that $\lambda_0 = L_y$). For L_y comparable or slightly larger than λ_m, the pattern length increases linearly for very long times. However, for L_y smaller than λ_m, the dynamics is significantly modified: The growth is suppressed, and it even saturates for small $L_y \approx \lambda_c$ [see Fig. 2(c)]. This slowing down of the growth for $L_y < \lambda_m$ points to a nontrivial behavior of the system close to the bifurcation point $L_y = \lambda_c$. For $D=0$, $L_y \approx \lambda_c$ appears to be a requirement for the growth saturation and for the existence of a nontrivial traveling wave. For $D>0$, however, our numerical results imply that this traveling wave solution is always admissible. A natural question to ask is whether there is something special about the $D=0$ case, and whether arbitrary small D is sufficient to modify the long time dynamics. The answer to this question cannot be

accurately reached based on numerical results alone, and will be subject of our future work [see also Remark (1) below].

To return now to comparison with the results reported in Ref. 20, we note that the related simulations reported there are performed using $L_y \approx 12$ and $b = 0.05$. From Fig. 11(a), one can already anticipate that the range of L_y's, for which growth stops, broadens as b is increased. This has been confirmed by additional simulations. In particular, these simulations show that, for the parameters as in Ref. 20, growth saturation occurs. Correspondingly, the results presented here and in that work are consistent. However, the fact that the results are qualitatively modified as the parameters (L_y and b) are changed, shows that one has to be very careful with reaching any general conclusions concerning long time behavior of the flow. We note that in most of the laboratory experiments, the domains are large, and b's are small. From our results, it follows that one should not expect growth saturation in the laboratory experiments of the flow down a vertical plane. Still, further research of this problem, both theoretical and experimental, is definitely required.

Remarks:

(1) From the discussion in this section, it is obvious that the saturation effect, and, in particular, the saturated length of the patterns, depends on a number of factors, most important being D, b, and L_y. Our results for different D's shown in Fig. 10 are obtained using a particular combination of $[L_y, b]$, and depend on these two parameters. Despite this limitation, we consider that it is of interest to find the functional dependence of the pattern length on the value of D (i.e., the inclination angle, assuming all other parameters are fixed). For this reason, we have performed additional simulations, for D's in the range $[0,1]$, with the idea of estimating the pattern length for $D \to 0$ by extrapolation. We find that best agreement is provided by the power law: $L(t \to \infty) = CD^{-\beta}$, with $C \approx 25.74$ and $\beta \approx 1.46$. We note that this fitting function slightly overestimates the pattern lengths for larger D's ($D > 1$), while it approximates very well the results for smaller D's. This fit predicts an infinite length for $D = 0$, i.e., flow down a vertical plane. Future experiments shall verify this prediction.

(2) An increase of L_y above λ_m (but still requiring $\lambda_0 = L_y$), leads to a completely different effect. From LSA, we know that the growth rates of longer wavelengths are being significantly reduced [see Fig. 2(c) for $\lambda > \lambda_m$]. Correspondingly, one expects that for a sufficiently large L_y, nonlinear mode (self) interaction can lead to emergence of new modes, that are not imposed initially. Figure 12 shows precisely this effect. As L_y is increased, new modes develop. These modes are characterized by shorter (and more unstable) wavelengths, i.e., separations between fingers. The particular mode that emerges is determined by the domain size. In Fig. 12 we show three examples where the resulting modes are given by $\lambda = L_y/2$ for $L_y = 24$ in Fig. 12(a) and $L_y = 32$ in Fig. 12(b), and by $\lambda = L_y/4$ for $L_y = 48$ in Fig. 12(c). [Note that the y scales in the parts (a)–(c) of this figure are different. In particular, the widths of the emerging fingers are the same in all cases shown.] Since our computations require $\partial h / \partial y = 0$ at the domain boundaries ($y = 0, L_y$), and the ini-
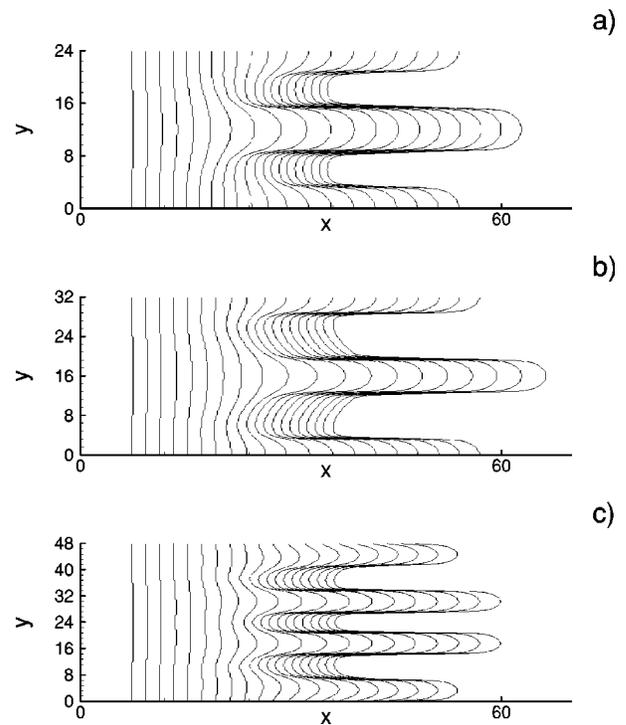
FIG. 12. Snapshots of the contact line at $\delta t = 2$ intervals for $L_y = \lambda_0 = 24$ (a), $L_y = \lambda_0 = 32$ (b), and $L_y = \lambda_0 = 48$ (c). All other parameters are as in Fig. 4.

tial condition is symmetric with respect to the domain center ($y = L_y/2$), these newly produced wavelengths are constrained by the approximate requirement $\lambda \approx L_y/i$, $i = 2,3,\dots$ (This requirement is approximative because not all emerging λ's in any given simulation have to be the same. However, they are typically close to λ_m.) We note that Fig. 12 shows a slightly faster growth of the finger in the middle of the domain for $L_y = 32$ [Fig. 12(b)], compared to the one for $L_y = 24$ [Fig. 12(a)]. This can explained based on the larger growth rate for $\lambda = 16$, compared to $\lambda = 12$. The fingers centered around $y = L_y/2$ grow faster in both cases than those at $y = 0, L_y$, since they develop directly through the linear growth mechanism from the initially imposed perturbations. Figure 12(c) differs because the initially imposed perturbation is completely removed; consequently, the growth of the resulting patterns is slower. More discussion concerning nonlinear mode interaction follows in Sec. IV.

(3) The long time dynamics can be also influenced by the size of the computational domain in the x direction. We observe in the simulations that if the length of the pattern, $L(t)$, becomes comparable to L_x, the saturation can occur. One possible interpretation is that if $L(t) \approx L_x$, only a small part of the main body of the fluid is kept inside the domain, leading to a modified dynamics. The results we present here for $D = 0$ case are calculated using $L_x = 200$; the (linear) growth of the pattern is followed until $t = 240$. If smaller box size, i.e., $L_x = 100$ is used, we observe the deviation from linear growth at $t \approx 130$, when $L(t) \approx 90$.

(4) The influence of the size of b on instability for the flow down an inclined plane is similar to that of the flow down a vertical plane, with possibly less dramatic consequences since the shape of the patterns is already triangular
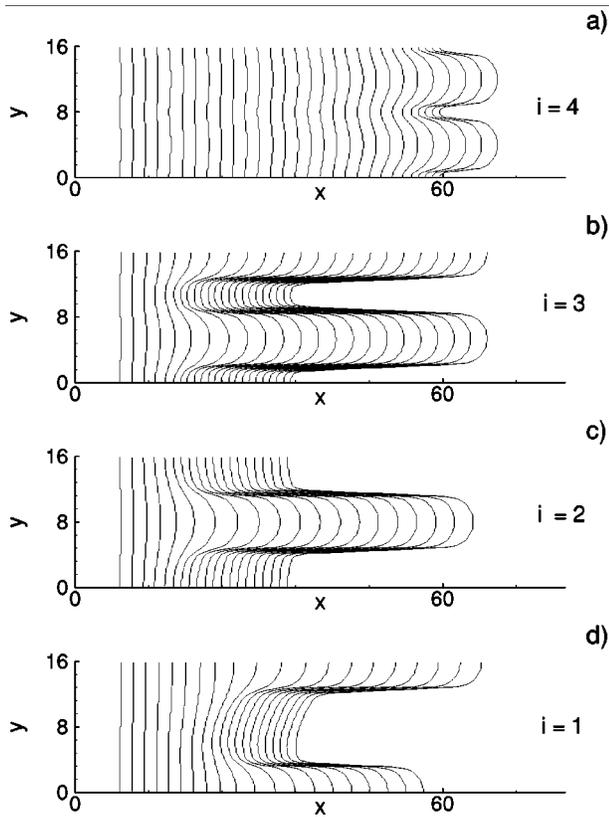
FIG. 13. Snapshots of the contact lines at $\delta t = 2$ intervals for four different perturbations: $\lambda_{0,i} = 2L_y/i$, $i = 4,3,2,1$ for (a)–(d), respectively. All other parameters are as in Fig. 4.

FIG. 14. (a) Snapshots of the contact line at $\delta t = 2$ intervals where initially more than one mode is present ($\lambda_{0,i} = 2L_y/i$). (a) $i = 1,2$, (b) $i = 1,4$, (c) $i = 1,2,3,4$. All other parameters are as in Fig. 4.

V. NONLINEAR MODE INTERACTION

In the first part of this section, we still analyze a narrow system, characterized by $L_y \approx \lambda_m$, but with a few modes initially present. This configuration allows to gain better insight into the nonlinear mode interaction. In the second part of this section, Sec. IV B, we extend the discussion to large systems, where $L_y \gg \lambda_m$, so that the results can be directly compared to experiments.

A. Narrow domain: $L_y \approx \lambda_m$

To simplify the discussion, here we consider only the flow down a vertical plane ($D = 0$). Figures 13 and 14 show an example of how the initial perturbation influences the development of instability. We still use $L_y = 16$, but impose perturbations characterized by different $\lambda_{0,i} = 2L_y/i$, $i = 1,2,3,4$ (these wavelengths are permitted by the boundary conditions at $y = 0, L_y$). For $i > 4$, the resulting perturbations are characterized by $\lambda_{0,i} < \lambda_c$ from LSA [see Fig. 2(c)], and they die away for very short times, resulting in a straight contact line.

Figure 13 shows the evolution when only one mode is initially present. Figure 13(a) shows the slow growth of a weakly unstable mode $\lambda_0 = 8$; Figs. 13(b) and 13(c) follow the growth of more unstable modes $\lambda_0 = 32/3, 16$. All these results are as expected from LSA; the only difference between them is in their growth rates. Figure 13(d), on the other hand, shows the effect of the nonlinearity on the development of the instability. Initially, only the mode $\lambda_0 = 32$ is present, with peak at $y = 16$. This mode is, however, very weakly unstable, and leaves enough space in the domain for other unstable modes to develop, similarly to the results

(viz. Fig. 7 for $D = 0$ case). Larger b's lead to decreased instability, as expected. We note that for larger values of D, the instability can be completely suppressed by using a thick precursor film, in agreement with the weakly nonlinear result by Kalliadasis,[16] and with experimental results by Veretennikov et al.[5] and Ye and Chang[17] for the flow down a (prewetted) inclined plane. In particular, based on LSA in the limit of small wave numbers, it is shown that one can define a stability boundary in $[D,b]$ space, that separates stable from unstable situations.[17] They obtain $D_{crit} = -C \log b$, where $C = 0.88$. This logarithmic dependence is consistent with the general statement that the macroscopic fluid behavior depends in a logarithmic way on any small length scale introduced at the contact line.[10,26,35] Interestingly enough, despite the fact that our simulations solve the fully nonlinear problem for larger wave numbers, we recover approximately logarithmic behavior as in Ref. 17, with a similar value of C.

(5) In this work, we do not discuss the development of instability for very small inclination angles, such as $\alpha = 1.8°$ in Johnson et al.,[8] 4° in de Bruyn,[4] or 8° in Ye and Chang.[17] Experimentally, instability is observed for these inclination angles; on the other hand, LSA predicts stability.[15] Ye and Chang[17] suggest that the continuous spectrum of the linear operator governing the dynamics in the linearized version of Eq. (5) has to be included to properly account for the influence of the surface inhomogeneities. Our work on addressing this problem is in progress.

shown in Fig. 12. In this particular case, the boundary conditions dictate development of the mode $\lambda=16$. The initially imposed asymmetry of the problem (with respect to the $y=8$ line) results in an asymmetric situation for longer times, with the pattern at $y=16$ ahead of the one at $y=0$.

Figure 14 shows snapshots of the contact line where more than one mode is superimposed at $t=0$ in the domain of width $L_y=16$. In Fig. 14(a), modes $\lambda_0=16,32$ are initially present; we see that the mode with larger growth rate ($\lambda=16$ in this case) wins, while the weakly unstable mode $\lambda=32$ completely disappears. The initial asymmetry reflects itself only in a small shift of the pattern to larger y's [compare with Fig. 13(c)]. Figure 14(b) shows an example of a situation where two initially present, weakly unstable modes $\lambda_0=8,32$, completely disappear, while the asymmetric mode $\lambda=16$ appears. In Fig. 14(c) we follow the competition of all four modes. The outcome is similar to Fig. 13(b) where only the mode $\lambda_0=32/3$ is initially present; however, the presence of other modes (in particular, $\lambda_0=16$) leads to a modified growth of the pattern centered around $y\approx7$.

Obviously, more work is needed to understand the mode interaction on a more fundamental level. Weakly nonlinear analysis, presented recently by Kalliadasis[16] is a promising starting point in this direction. The main purpose of the discussion presented here is to illustrate the nonlinear mode interaction, and to provide some insight into experimentally observed patterns. For example, one question raised by experiments is the source of nonuniform distribution of patterns, and their unequal length.[1,4,8,36] Here, we see that these effects can be a consequence of the nonlinear interaction of just a few modes, limited to a narrow computational domain.

B. Wide domain: $L_y \gg \lambda_m$

In this section we present results for the instability in wide domains, whose size compares well with the experimental ones. We model experimental noise by modifying the position of the fluid front through a perturbation of the form

$$x_f(y) = x_{f0} - \sum_{i=1}^{N} A_i \cos(2\pi y/\lambda_{0,i}), \qquad (16)$$

where $\lambda_{0,i}=2L_y/i$ as explained above, and A_i is the amplitude of the ith mode, chosen randomly in the range $[-0.1,0.1]$. In the limit $N\to\infty$, this initial condition is the Fourier expansion of a smoothly corrugated contact line. The simulations are typically performed using $L_y=96$, $N=50$, and $\Delta y=0.5$. Additional simulations confirm that the main features of the results are independent of the domain size, the grid resolution, and the number of modes imposed at $t=0$.

Figure 15 shows the snapshot of the contact line as the fluid film flows down a vertical plane (see Ref. 21 for the contour plots). In agreement with LSA[14,15] and experiments,[4,8] the short λ's disappear quickly, since these are linearly stable. For later times, long finger-like rivulets form, as reported by Johnson[7] and Johnson et al.[8] (see also Fig. 1). The emerging λ's (separation between the fingers) are close to λ_m. However, LSA applies only to short times and cannot predict the behavior of the system when the perturbations become large. At this point, nonlinear simulations are the
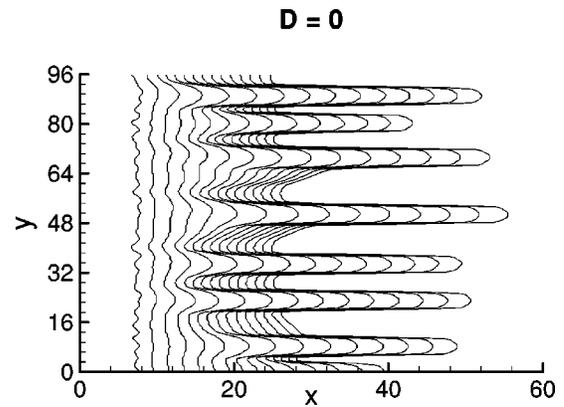
FIG. 15. Snapshots of the contact line in $\delta t=2$ intervals for the flow down a vertical plane ($L_y=96$, $N=50$, $b=0.01$, $\Delta x=0.2$, $\Delta y=0.5$).

only means of linking experiments with theory. Indeed, inspection of Fig. 15 recovers results which compare favorably with experimental ones. One of these results is a natural nonuniformity of the emerging λ's—the system chooses the most favorable configuration, that results from the nonlinear coupling between the initially present modes, modified by the limitations imposed by a finite system size. Similar spread of emerging λ's is also observed experimentally, in both constant volume and constant flux configurations.[4,6,8] Furthermore, coarsening effects can be seen in Fig. 15 (e.g., compare the profiles at $t=10$ and $t=30$ for $y\approx70$). If two fingers initially start developing too close to each other, the large curvature in the y direction apparently forces them to merge. We note that the tips of the fingers for late times move with constant velocity that is larger than the (constant) velocity of the roots (compare the distance between two consecutive snapshots in Fig. 15). Correspondingly, there is no growth saturation, similarly to the narrow domain and large λ_0 results from Sec. III A.

Figure 16, where $L_y=192$, shows that an increase in domain size does not significantly influence the development
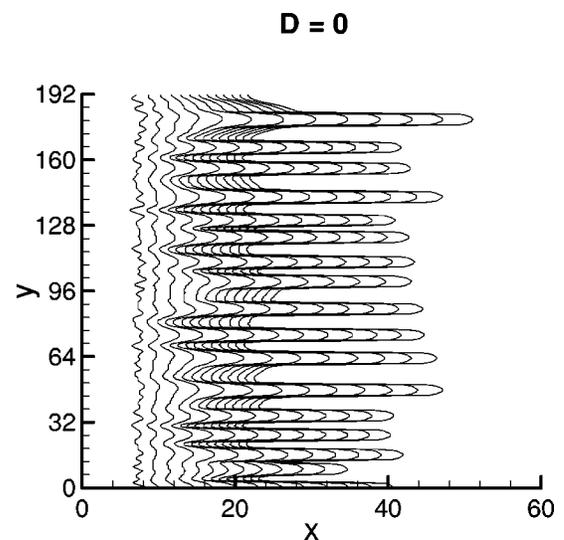
FIG. 16. Snapshots of the contact line in $\delta t=2$ intervals for the flow down a vertical plane ($L_y=192$, $N=100$). All other parameters are as in Fig. 15.

D = 0   **h**

FIG. 17. 3D contour plot of the fluid at the last time shown in Fig. 15.

D = 0, b = 0.1
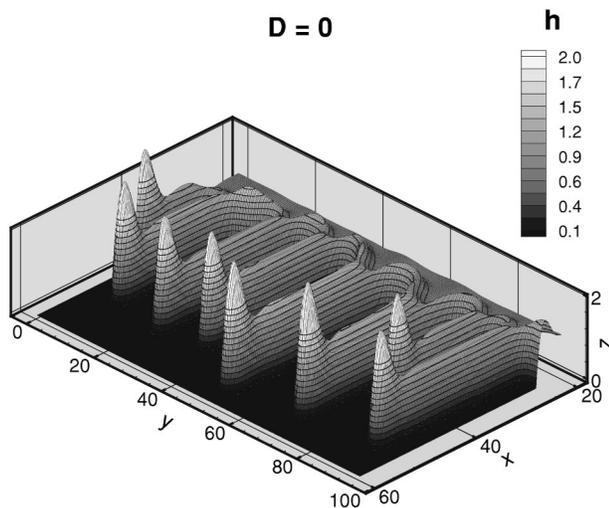
FIG. 18. Snapshots of the contact line in $\delta t = 2$ intervals for the flow down a vertical plane. Here $b = 0.1$; all other parameters are as in Fig. 15.

of instability. There is still a relatively large spread of emerging wavelengths, as in Fig. 15. Careful inspection of Fig. 16 shows, however, an additional effect. The patterns that develop closely spaced are characterized by a slower growth (e.g., the patterns about $y \approx 32, 128, 160$, in Fig. 16). Similar effect can be also seen in the experimental results shown in Fig. 1. An explanation of this effect follows by extension of the narrow domain results from Sec. IV to this setting. Figure 11(b) shows that for small L_y, growth rates decrease. What governs the growth rate of individual fingers in Fig. 16 appears to be the distance to the neighbors; this distance plays the same role as the domain size in Fig. 11(b). Alternatively, this effect can be explained by a conservation of mass argument. The length of a pattern depends on the width of the region that supplies the fluid: Thus if patterns are close, each of them has less fluid available for its growth.

Figure 17 shows a 3D contour plot of the fluid at the last time shown in Fig. 15. The thickness of the fluid is much larger at the tips, while the capillary ridges are much smaller at the roots. Cross sectional profile of the fingers can be closely approximated by a cylindrical cap, similarly to the profiles obtained in narrow domains, see Diez and Kondic.[21]

Since some experiments are performed on a prewetted plane with different values of the precursor thickness (e.g., Veretennikov et al.[5]), it is of interest to see how different b's influence our results in the case of large L_y. This result is shown in Fig. 18. A large precursor leads to emerging patterns that are more rounded compared to the $b = 0.01$ case (see Fig. 15), and their growth is much slower, as expected based on the simulations in narrow computational domains. Further, the average distance between the patterns is increased, as anticipated from LSA results, which show a shift of the mode of maximum growth towards longer wavelengths as b is increased.[14,15,24] The shapes of the patterns in this figure are similar to the ones obtained by Kalliadasis[16] using weakly nonlinear analysis for a similar value of b. As pointed out by the author, his approach is not valid for small b's, so the computational results obtained using $b = 0.01$ (e.g., Fig. 15) cannot be directly compared to his results.
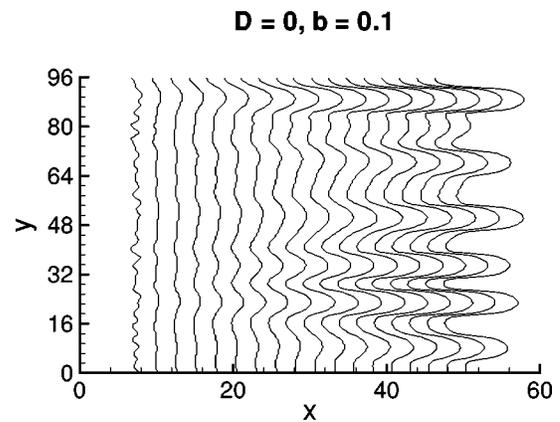
Next, we proceed to model the flow down an inclined plane. Figure 19 shows the representative case $D = 1$ (see also Ref. 21). The emerging patterns strongly resemble the experimental results shown in Fig. 1 for $\alpha < 90°$. Their shape is now triangular, and the roots are almost shrunk to a point. The growth of the patterns is slower compared to $D = 0$, and their separations and widths are increased, even in terms of the length scale $x_c(\alpha)$ (note that Fig. 19 shown the snapshots in $\delta t = 5$ intervals, compared to Fig. 15 where $\delta t = 2$).

Examination of Fig. 19 for late times shows that a steady-state configuration has been reached. This result says that the growth saturation is not an effect related to artificially narrow computational domains (Sec. IV), but it also appears in domains that compare well with the experimental ones (such as the one shown in Fig. 1). Future careful experiments should give a definite answer to the questions related to the existence of nontrivial traveling waves.

Figure 20 shows the 3D fluid profile for this case. The capillary ridges are much less pronounced compared to the flow down a vertical plane (viz. Fig. 17). We also note the formation of valleys across the emerging patterns, as observed by Johnson et al.[8]

It is interesting to observe that both an increase of D and an increase of b influence the emerging wavelengths in a

D = 1
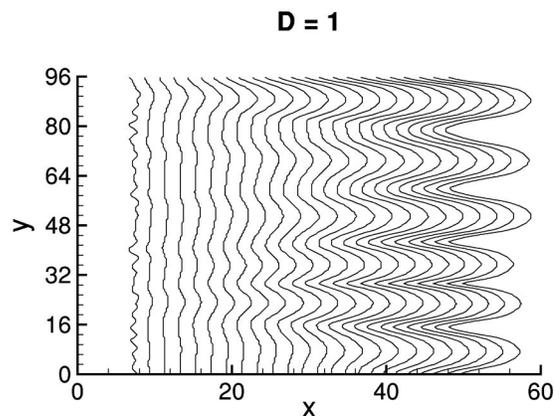
FIG. 19. Snapshots of the contact line for the flow down an inclined plane $D = 1$ in $\delta t = 5$ intervals. All other parameters are as in Fig. 15.
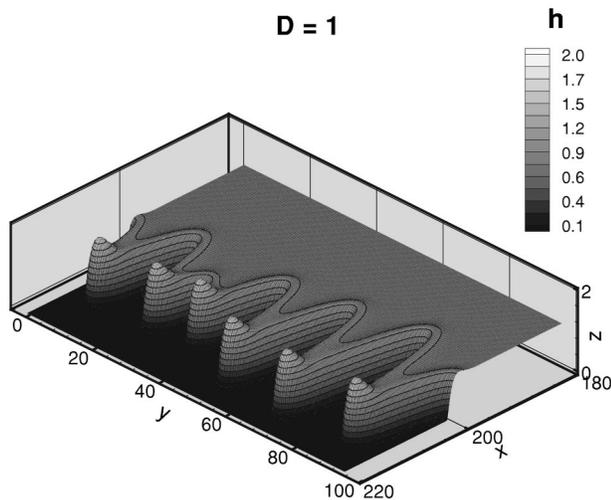
FIG. 20. 3D contour plot of the fluid at the last time shown in Fig. 19.

TABLE II. The table gives inclination angle α, nondimensional parameter D, calculated in-plane length, x_c, computed wavelengths of the patterns, λ_{comp}, experimentally measured wavelengths, λ_{exp} [from Johnson *et al.* (Ref. 8)] computed widths of the patterns, W_{comp}, and experimentally measured widths, W_{exp}, from Johnson (Ref. 7) [the widths for $\alpha=27.9°$ and $13.9°$ are also given in Johnson *et al.* (Ref. 8)]. Computed results report the average and one standard deviation; experimental results give average and reported/estimated uncertainty. All lengths are given in centimeters.

α	D	x_c	λ_{comp}	λ_{exp}	W_{comp}	W_{exp}
90°	0	0.15	1.8±0.4	2.0±0.3	0.8±0.1	0.7±0.1
27.9°	0.67	0.21	3.2±0.4	3.0±0.4	2.1±0.2	2.0±0.2
13.9°	1.34	0.28	4.5±0.5	4.0±0.5	3.2±0.2	3.0±0.3

similar fashion: In both cases, the typical emerging λ increases. Other characteristics of the emerging patterns are, however, very different, in particular the shape, and the widths of the roots.

From additional simulations similar to the ones shown in Figs. 15 and 19 (but characterized by different domain sizes and different seeds for the random number generator), we extract results for the average λ's, and for the widths, W's, of the patterns (full width at half length). These are computed at late times, when they are almost time independent. We obtain

$$\lambda_{D=0}=11.8\pm2.6, \quad \lambda_{D=1}=16.0\pm2.7, \tag{17}$$

where the average and one standard deviation are reported. The trend of increase of the emerging wavelengths as D is increased is consistent with LSA. The average values are smaller than predicted by LSA ($\lambda_m\approx14$ for $D=0$[14]); however, the difference is less than one standard deviation. Assuming that this difference is real, the results of Sec. IV A suggest that the nonlinear interaction among the competing normal modes is responsible; nevertheless, we believe that further research is needed to completely clarify this issue. We note that recently, Ye and Chang[17] analyzed the effect of noise generated in the prewetted surface on the emerging wavelengths, and also observed the emergence of wavelengths shorter than predicted by LSA. That work, however, is concerned with the constant volume flow, where thinning of the fluid may have important consequences [see also Remark (5) below].

The widths of the patterns are given by

$$W_{D=0}=5.5\pm0.4, \quad W_{D=1}=11.2\pm1.0. \tag{18}$$

We note a significant increase of W's as D is increased. Also, W's are much more uniform than λ's, as observed in the experiments.[4,8]

In order to directly compare computational results with experimental ones, we now proceed to model a particular experimental situation. We concentrate on the works by Johnson[7] and Johnson *et al.*[8] that report experimental results concerning the influence of the inclination angle α on the shape of the patterns in a constant flux flow. Their results

(one example is reproduced in Fig. 1) show a well defined transition from rounded triangular patterns for small α to finger-like rivulets for the vertical plane, in complete agreement with the computational results presented here. To facilitate a quantitative comparison with these experiments, we have performed additional simulations with the particular set of parameters used in Refs. 7 and 8. We choose to model "Fluid B" as reported in Ref. 8, since it is characterized by a small contact angle. This fluid (80% glycerin in water) has density $\rho=1.21$ g/cm^3, kinematic viscosity $\nu=0.69$ cm^2/s, and surface tension $\gamma=66$ dyn/cm. The inclination angles that we reproduce here are $\alpha=90°$, 27.9°, and 13.9°. The thickness of the fluid far behind contact line is not directly reported for all inclination angles; however, we can obtain this quantity from the reported value of Reynolds number, Re, which is defined as $Re=Q/\nu$, where Q is the volumetric flow rate per unit width. This gives $h_c=[3Re\,\nu^2/(g\sin\alpha)]^{1/3}$, so we obtain $h_c=0.057$, 0.074, 0.092 (cm) for $\alpha=90°$, 27.9°, 13.9°, respectively. Using Eq. (4) we calculate the corresponding length scales and D's for these three angles; see third column of Table II. We note that the results presented Refs. 7 and 8 show very little dependence on Reynolds number, implying that the inertial effects play only minor role in that experimental setup.

Figure 21 shows contour plots of the finger profiles for these three angles when the fronts have traveled the same distance down the incline. The results in this figure are given in dimensional units, using the scales obtained above, so that they can be compared to the experiment shown in Fig. 1. We note that the direct comparison is limited by a few factors: (1) The width of our computational domain is about a half of the experimental one; (2) the initial conditions are different, since the size of the initially imposed perturbations in the simulations is much larger than any microscopic noise present in the experiment, and (3) the experimental results are shown at much later times, leading to longer patterns than those shown in Fig. 21. (Note the patterns shown in Fig. 21 have not yet reached their saturation lengths.) Still, the main features of the results agree very well. In both experiment and simulations there is a clearly defined transition from rounded triangular patterns for smaller inclination angles to finger-like rivulets for the vertical plane. As D is increased, the instability is weaker, both in experiments and computations. Also, the emerging wavelengths increase.

The length scale x_c (third column in Table II) allows for
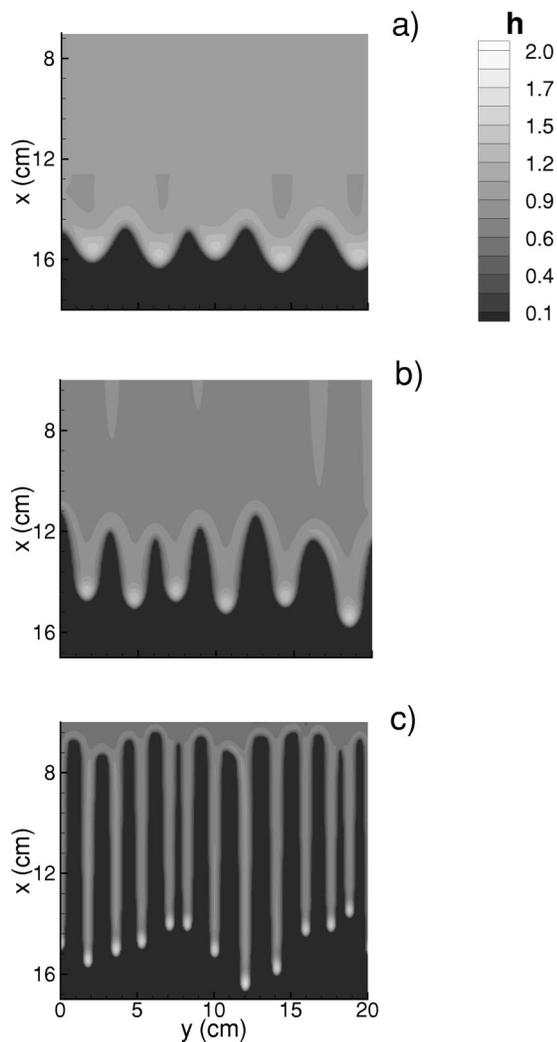
FIG. 21. Contour plots of fluid profiles for (a) $D=0$; (b) $D=0.67$, and (c) $D=1.34$, plotted when the fluid traveled the same distance downslope. All other parameters are as in Fig. 15. Note that the x and y scales are in cm, and fluid thickness, h, is in mm.

a more quantitative comparison between the computed and experimental results. We calculate the average dimensional wavelengths and widths of the patterns, and compare them directly with the experimental results shown in Fig. 1. Table II shows that the agreement of the calculated and experimental values is remarkably good.

Remarks:

(1) In this section, we do not discuss in detail the issues related to length saturation, since the main features of the results are similar to the ones discussed in Sec. IV.

(2) As noted above, the dimensional wavelengths are also increasing as α is decreased. From Table II, the average values for these wavelengths are given approximately by $\lambda=12,15,16$ for $\alpha=90°$, 27.9°, 13.9°, respectively. So, α significantly influences the emerging wavelengths, at least in the constant flux case. This is in contrast to the experiments by Huppert,[2] performed with a constant fluid volume, which suggest that (dimensionless) λ's should not depend on inclination angles.

(3) The results for average λ's reported in Table II do not

depend on the domain size, and the relatively large spread of λ's is not being reduced as the domain size is increased. This shows that the experimentally observed spread of λ's is not due to, e.g., boundary effects, but it is an intrinsic property of the system.

(4) Based on the constant volume experimental results, Jerret and de Bruyn[3] predict that the pattern width scales as $W\sim(\sin\alpha)^{-0.66}$. This fit, however, does not appear to be consistent with neither experimental results by Johnson *et al.*,[8] nor the computational results presented here, showing another significant difference between constant volume and constant flux configurations.

(5) In this work, we analyze the instabilities that develop after the contact line–fluid front is perturbed. In physical experiments, triggering perturbations could be also propagating from the precursor film in front of the main body of the fluid. These perturbations were analyzed recently by Ye and Chang.[17] That work, however, addresses very different setup where constant volume of the fluid is assumed, so that the fluid is thinning behind the front as time progresses. This thinning introduces additional set of effects that are beyond the scope of this work.

Now we briefly discuss the influence of the precursor perturbations in the constant flux case. From 1D simulations[22] we know that the height of the capillary ridge, which is related to instability development, can be modified by the perturbations of the precursor. Here we show that localized 2D perturbations could really lead to the onset of instability. To illustrate this point, Fig. 22 presents how the perturbations [shown in Fig. 22(a)] influence the unperturbed fluid film. These perturbations of the precursor are characterized by their extend in the x and y directions (2.0 ± 1.0), x coordinate (12 ± 1.0), the distance between the perturbations in the y direction (7 ± 1.0), and the depth $[(0.5\pm0.1)b]$. In addition there is a smooth transition region around each perturbation. The parameters are chosen randomly in the given range; we do not present here a systematic study of the influence of these parameters on the instability, but just show that the instability can be induced by this type of perturbations. They are distributed close to each other in the y direction in order not to perturb the system with the wavelengths close to the wavelength of maximum growth from LSA; by perturbing with relatively high-frequency noise, we force the system to decide on emerging wavelengths on its own.

The similarity of the emerging patterns presented in Fig. 22 and the earlier results obtained by perturbing the contact line (i.e., Fig. 15) clearly shows that the precise mechanism of imposing perturbations is not important. In particular, the emerging wavelengths (distance between the fingers) are approximately the same as obtained before [viz. Figs. 15, 16, and Eq. (17)]. Analogous results are obtained for flows on an incline, where $D\neq0$. We emphasize that constant volume flow on real surfaces, where (i) fluid is continuously perturbed and (ii) fluid is thinning, opens additional set of questions related to the positioning of the perturbations, as pointed out in Ref. 17. We will address this questions elsewhere.

Phys. Fluids, Vol. 13, No. 11, November 2001

Pattern formation in the flow of thin films   3183

(a)

(b)
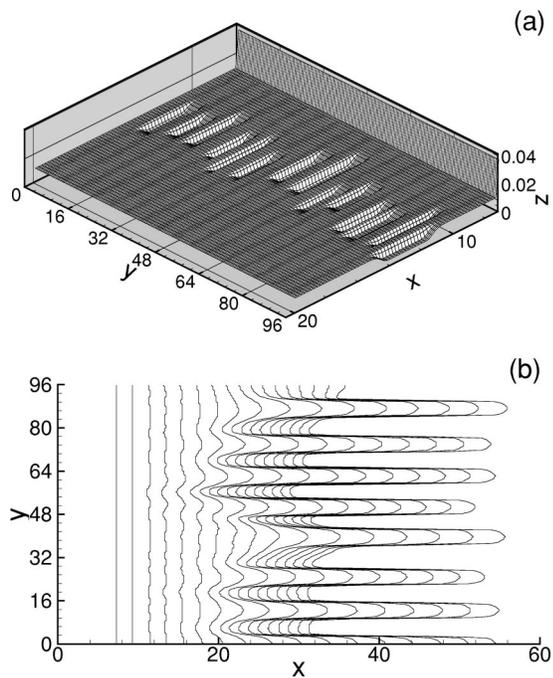
FIG. 22. Flow over perturbed precursor. Part (a) shows (magnified) region of the precursor region that is perturbed; the front of the main body of the fluid is shown to the right (around $x \approx 7$). Note that the scale of the plot is significantly extended in the x direction relative to y; average shape of the perturbations is circular. Part (b) shows the snapshots of the contact line at $\delta t = 2$ intervals. Note the similarity to the results shown in Fig. 15. All the parameters are as in Fig. 15, except for the pertubations of the contact line, that are absent here.

VI. CONCLUSION

Through series of computations, we have obtained results for the wavelengths and profiles of the patterns that develop when a completely wetting fluid flows down an incline. The agreement with experiments is remarkably good, showing that the lubrication model with a precursor film captures the most important physical mechanisms that determine the origin of the instability.

There are two main conclusions of this work. First, the inclination angle significantly influences the stability of the contact line in the case of spreading of a completely wetting fluid on an inclined plane. Large inclination angles lead to fingers with almost straight sides, while smaller inclination angles lead to patterns with much more oblique sides, resembling experimentally observed saw-tooth patterns. Second, the question of surface coverage is not necessarily related to the shape of the emerging patterns. In all of our simulations, the roots of the patterns move, leading to a complete surface coverage. The shape of the patterns can, however, vary considerably. This result implies that partially wetting fluid is required for partial surface coverage, in agreement with a number of experimental observations. The (triangular) shapes of the patterns that are obtained in the experiments which use wetting fluids are, however, influenced not only by the fluid wetting properties, but also by (usually small) inclination angles of the substrate.

Another interesting result of our computations is the indication that a nontrivial traveling wave solution may exist

for the flow down an inclined plane, with the steady-state lengths of the pattern depending on the precise values of the flow and fluid parameters. It would be of interest to perform careful experiments to verify this prediction. Complementary theoretical research should show existence and stability of these steady solutions. Our computational observation that the existence of these solutions depends on the parameter $D(\alpha)$, and on the size of the computational domain, implies a rich structure of this dynamical system that should be analyzed in a more fundamental manner. The results presented here provide useful guidance in this direction.

In this work, we concentrate on the situation where the fluid thickness is kept constant far behind the apparent contact line, since this configuration allows for understanding of many features of the problem without the additional complication introduced by the thinning of the fluid in the constant volume case. In the present case, we show that the exact mechanism of imposing perturbations in the system is not of major importance; in particular, we obtain similar emerging wavelengths independently on whether we perturb contact line, or the precursor film. We continue our research of both constant volume case, and of the dynamics of partially wetting fluids, with the hope of understanding the interplay between fluid wetting properties, gravity, and fluid thinning that determines the nature of the instability and the surface coverage.

[1] N. Silvi and E. B. Dussan V, "On the rewetting of an inclined solid surface by a liquid," Phys. Fluids **28**, 5 (1985).
[2] H. Huppert, "Flow and instability of a viscous current down a slope," Nature (London) **300**, 427 (1982).
[3] J. M. Jerrett and J. R. de Bruyn, "Finger instability of a gravitationally driven contact line," Phys. Fluids A **4**, 234 (1992).
[4] J. R. de Bruyn, "Growth of fingers at a driven three-phase contact line," Phys. Rev. A **46**, R4500 (1992).
[5] I. Veretennikov, A. Indekina, and H.-C. Chang, "Front dynamics and fingering of a driven contact line," J. Fluid Mech. **373**, 81 (1998).
[6] L. M. Hocking, W. R. Debler, and K. E. Cook, "The growth of leading-edge distortions on a viscous sheet," Phys. Fluids **11**, 307 (1999).
[7] M. F. G. Johnson, Ph.D. thesis, Northwestern University, 1997.
[8] M. F. G. Johnson, R. A. Schluter, and S. G. Bankoff, "Experimental study of rivulet formation on an inclined plate by fluorescent imaging," J. Fluid Mech. **394**, 339 (1999).
[9] E. B. Dussan V, "On the spreading of liquids on solid surfaces: Static and dynamic contact lines," Annu. Rev. Fluid Mech. **11**, 317 (1979).
[10] P. G. de Gennes, "Wetting: Statics and dynamics," Rev. Mod. Phys. **57**, 827 (1985).
[11] P. J. Haley and M. J. Miksis, "The effect of the contact line on droplet spreading," J. Fluid Mech. **223**, 57 (1991).
[12] R. Goodwin and G. M. Homsy, "Viscous flow down a slope in the vicinity of a contact line," Phys. Fluids A **3**, 515 (1991).
[13] P. G. López, M. J. Miksis, and S. G. Bankoff, "Inertial effects on contact line instability in the coating of a dry inclined plane," Phys. Fluids **9**, 2177 (1997).
[14] S. M. Troian, E. Herbolzheimer, S. A. Safran, and J. F. Joanny, "Fingering

instabilities of driven spreading films," Europhys. Lett. **10**, 25 (1989).

[15]A. L. Bertozzi and M. P. Brenner, "Linear stability and transient growth in driven contact lines," Phys. Fluids **9**, 530 (1997).

[16]S. Kaliadakis, "Fingering phenomena for driven coating films," J. Fluid Mech. **413**, 355 (2000).

[17]Y. Ye and H. Chang, "A spectral theory for fingering on a prewetted plane," Phys. Fluids **11**, 2494 (1999).

[18]L. W. Schwartz, "Viscous flows down an inclined plane: Instability and finger formation," Phys. Fluids A **1**, 443 (1989).

[19]D. T. Moyle, M. S. Chen, and G. M. Homsy, "Nonlinear rivulet dynamics during unstable dynamic wetting flows," Int. J. Multiphase Flow **25**, 1243 (1999).

[20]M. H. Eres, L. W. Schwartz, and R. V. Roy, "Fingering phenomena for driven coating films," Phys. Fluids **12**, 1278 (2000).

[21]J. Diez and L. Kondic, "Contact lines instability of thin liquid films," Phys. Rev. Lett. **86**, 632 (2001).

[22]L. Kondic and A. L. Bertozzi, "Nonlinear dynamics and transient growth of driven contact lines," Phys. Fluids **11**, 3560 (1999).

[23]H. P. Greenspan, "On the motion of a small viscous droplet that wets a surface," J. Fluid Mech. **84**, 125 (1978).

[24]M. A. Spaid and G. M. Homsy, "Stability of Newtonian and viscoelastic dynamic contact lines," Phys. Fluids **8**, 460 (1996).

[25]M. P. Brenner, "Instability mechanisms at driven contact lines," Phys. Rev. E **47**, 4597 (1993).

[26]E. B. Dussan V, "The moving contact line: the slip boundary condition," J. Fluid Mech. **77**, 665 (1976).

[27]L. M. Hocking and A. D. Rivers, "The spreading of a drop by capillary action," J. Fluid Mech. **121**, 425 (1982).

[28]J. Diez, L. Kondic, and A. L. Bertozzi, "Global models for moving contact lines," Phys. Rev. E **63**, 011208 (2001).

[29]L. Zhornitskaya and A. L. Bertozzi, "Positivity preserving numerical schemes for lubrication-type equations," SIAM (Soc. Ind. Appl. Math.) J. Numer. Anal. **37**, 523 (2000).

[30]L. Zhornitskaya, Ph.D. thesis, Duke University, 1999.

[31]F. Bernis and A. Friedman, "Higher order nonlinear degenerate parabolic equations," J. Diff. Eqns. **83**, 179 (1990).

[32]E. O. Tuck and L. W. Schwartz, "A numerical and asymptotic study of some third-order ordinary differential equations relevant to draining and coating flows," SIAM Rev. **32**, 453 (1990).

[33]L. H. Tanner, "The spreading of silicone oil drops on horizontal surfaces," J. Phys. D **12**, 1473 (1979).

[34]M. F. G. Johnson (private communication).

[35]E. B. Dussan V and S. Davis, "On the motion of a fluid-fluid interface along a solid surface," J. Fluid Mech. **65**, 71 (1974).

[36]L. M. Hocking, "Sliding and spreading of thin two-dimensional drops," Q. J. Mech. Appl. Math. **34**, 37 (1981).